Protein Science (1998), 7:2541–2549. Cambridge University Press. Printed in the USA.

The crystal structure of NADPH:ferredoxin reductase from *Azotobacter vinelandii*

G. SRIDHAR PRASAD,[1] N. KRESGE,[1] A.B. MUHLBERG,[1] A. SHAW,[1,3] Y.S. JUNG,[2] B.K. BURGESS,[2] AND C.D. STOUT[1]

[1]Department of Molecular Biology, The Scripps Research Institute, 10550 North Torrey Pines Road, La Jolla, California 92037-1093

[2]Department of Molecular Biology and Biochemistry, University of California, Irvine, California 92697-3900

(RECEIVED June 10, 1998; ACCEPTED August 7, 1998)

Abstract

NADPH:ferredoxin reductase (*Av*FPR) is involved in the response to oxidative stress in *Azotobacter vinelandii*. The crystal structure of *Av*FPR has been determined at 2.0 Å resolution. The polypeptide fold is homologous with six other oxidoreductases whose structures have been solved including *Escherichia coli* flavodoxin reductase (*Ec*FldR) and spinach, and *Anabaena* ferredoxin:$NADP^+$ reductases (FNR). *Av*FPR is overall most homologous to *Ec*FldR. The structure is comprised of a N-terminal six-stranded antiparallel β-barrel domain, which binds FAD, and a C-terminal five-stranded parallel β-sheet domain, which binds NADPH/$NADP^+$ and has a classical nucleotide binding fold. The two domains associate to form a deep cleft where the NADPH and FAD binding sites are juxtaposed. The structure displays sequence conserved motifs in the region surrounding the two dinucleotide binding sites, which are characteristic of the homologous enzymes. The folded over conformation of FAD in *Av*FPR is similar to that in *Ec*FldR due to stacking of Phe255 on the adenine ring of FAD, but it differs from that in the FNR enzymes, which lack a homologous aromatic residue. The structure of *Av*FPR displays three unique features in the environment of the bound FAD. Two features may affect the rate of reduction of FAD: the absence of an aromatic residue stacked on the isoalloxazine ring in the NADPH binding site; and the interaction of a carbonyl group with N10 of the flavin. Both of these features are due to the substitution of a conserved C-terminal tyrosine residue with alanine (Ala254) in *Av*FPR. An additional unique feature may affect the interaction of *Av*FPR with its redox partner ferredoxin I (FdI). This is the extension of the C-terminus by three residues relative to *Ec*FldR and by four residues relative to FNR. The C-terminal residue, Lys258, interacts with the AMP phosphate of FAD. Consequently, both phosphate groups are paired with a basic group due to the simultaneous interaction of the FMN phosphate with Arg51 in a conserved FAD binding motif. The fourth feature, common to homologous oxidoreductases, is a concentration of 10 basic residues on the face of the protein surrounding the active site, in addition to Arg51 and Lys258.

Keywords: crystal structure; FAD; ferredoxin reductase; NADPH

Azotobacter vinelandii is a free-living diazotroph that is commonly found in the soil. NADPH:ferredoxin reductase (E.C. 1.18.1.2) was first observed in this organism as a spot on a two-dimensional (2D) electrophoresis gel that dramatically increased in size in response to disruption of the *fdxA* gene that encodes a protein designated ferredoxin I (FdI) (Morgan et al., 1988). FdI is a well-characterized M_r 13 kD acidic 7Fe protein containing $[3Fe\text{-}4S]^{+/0}$ and $[4Fe\text{-}4S]^{2+/+}$ clusters with reduction potentials at pH 7.8 of −425 and −647 mV, respectively (Stout, 1989; Iismaa et al., 1991).

Reprint requests to: C.D. Stout, Department of Molecular Biology, The Scripps Research Institute, 10550 North Torrey Pines Road, La Jolla, California 92037-1093; e-mail: dave@scripps.edu.

[3]Present address: Genencor International Inc., 925 Page Mill Road, Palo Alto, California 94304-1013.

The overexpression of an unknown protein due to the absence of FdI suggested a regulatory and/or functional relationship between the two proteins. At the same time, in spite of extensive study, a physiological function for FdI had not been identified. The unknown protein was characterized as NADPH:ferredoxin reductase (Isas & Burgess, 1994; Isas et al., 1995); it is a monomer of M_r 29 kD containing a noncovalently attached FAD, which is specifically reduced by NADPH with a reduction potential at pH 7.4 of −327 mV. The reduction occurs without production of a stable semiquinone. The gene encoding the *A. vinelandii* NADPH:ferredoxin reductase was cloned and sequenced and the protein was overexpressed (Isas et al., 1995). Database searches at that time revealed that the *A. vinelandii* protein was most similar to an NADPH:ferredoxin reductase from *Escherichia coli* that was encoded by a gene designated *fpr* (Bianchi et al., 1993). For that

reason the *A. vinelandii* gene was designated *fpr* and the protein product FPR (Isas et al., 1995). In this study, which compares the structures of the two proteins, the NADPH:ferredoxin reductases from the two organisms will be referred to as *Av*FPR and *Ec*FldR. In the structure determination of the protein encoded by the *E. coli fpr* gene, the enzyme is characterized as flavodoxin reductase (Ingelman et al., 1997).

At the time that *Av*FPR was identified, a great deal was already known both about the function of *Ec*FldR and how the *Ecfpr* gene was regulated. The *E. coli* protein is part of a system that activates a number of different enzymes involved in anaerobic metabolism and it appears to specifically transfer electrons from NADPH to flavodoxin. The *Ecfpr* gene is a member of the *soxRS* regulon: its expression is induced by intracellular superoxide as a result of cell exposure to oxidants such as paraquat (Liochev et al., 1994). By analogy, it was proposed that the *fpr* gene might be similarly regulated in *A. vinelandii*, and since then a number of common features have emerged. For example, a regulatory sequence upstream of *Avfpr* has been identified and it is 50% identical to the SoxS binding site upstream of *Ecfpr*. This sequence is responsible for the upregulation of *Av*FPR that was originally observed in the FdI^- deficient, *A. vinelandii* strain LM100 (Yannone & Burgess, 1997). A putative *A. vinelandii* regulatory protein that binds specifically to this SoxS-like sequence has also been identified but has not yet been characterized so its relationship to SoxS is not currently known. However, in parallel with the *E. coli* system *Avfpr* is activated by exposing *A. vinelandii* to paraquat, through the SoxS-like sequence, and introduction of *Avfpr* into *E. coli* results in regulation by SoxRS proteins (Yannone & Burgess, 1998). In spite of these similarities, one very important difference between the two proteins lies in their choice of redox partner, FdI in *A. vinelandii* (Isas & Burgess, 1994) and flavodoxin in *E. coli* (Bianchi et al., 1993). FdI interacts specifically with *Av*FPR (Isas & Burgess, 1994) and is a critical component of the oxidative stress response in *A. vinelandii*.

Both *Ec*FldR and *Av*FPR are members of a large class of $NADP^+$ or NAD^+ specific enzymes containing FAD or FMN cofactors, which participate in electron transfer reactions (Correll et al., 1993; Lu et al., 1994; Nishida & Miki, 1996; Ingelman et al., 1997). Altogether seven crystal structures of members of this protein family have now been solved. All of the structures display a FAD or FMN binding domain comprised of a six-stranded antiparallel β-barrel with capping α-helix, and a $NADP^+$ or NAD^+ binding domain containing a parallel β-sheet nucleotide binding fold. The primary sequences display conserved motifs for specific binding of FAD or FMN and $NADP^+$ or NAD^+, as well-conserved residues presumed to be involved in hydride transfer.

*Ec*FldR is required for reductive activation of ribonucleotide reductase and other enzymes (Bianchi et al., 1993). The structure has been solved at 1.7 Å resolution for the FAD bound enzyme (Ingelman et al., 1997). Spinach ferredoxin:$NADP^+$ reductase (FNR) contains FAD and is reduced by a [2Fe-2S] cluster containing ferredoxin in the terminal step of photosynthesis to produce NADPH. The structure has been solved and refined at 1.7 Å resolution (Karplus et al., 1991; Bruns & Karplus, 1995) and in complex with 2′-phospho-5′-AMP (P-AMP) in the oxidized and reduced states at 1.7 and 2.0 Å (Bruns & Karplus, 1995). The FNR from the cyanobacterium *Anabaena* also transfers electrons from a 2Fe ferredoxin to $NADP^+$ and contains FAD; the structure has been solved at 1.8 Å resolution and at 2.25 Å in complex with $NADP^+$ (Serre et al., 1996). The FAD containing fragment of corn nitrate reductase (NiR) is a member of the family that utilizes NAD^+ and reduces cytochrome b5. The structure has been solved and refined at 2.5 Å (Lu et al., 1994, 1995) and in complex with ADP at 2.7 Å (Lu et al., 1995). A closely related porcine cytochrome b5 reductase (B5R) also containing NAD^+ has been solved at 2.4 Å resolution (Nishida et al., 1995). A sixth member of the family with known structure is the *Pseudomonas cepacia* phthalate dioxygenase reductase (PDR), which utilizes FMN and NAD^+. The structure has been solved at 2.0 Å resolution and in complex with NAD^+ and NADH at 2.7 Å (Correll et al., 1992). In this case a 2Fe ferredoxin that reduces the FMN, analogous to reduction of FAD in spinach and *Anabaena* FNR, is an attached carboxy terminal domain.

These structural analyses have defined the FAD or FMN binding sites and characterized the $NADP^+$ and NAD^+ binding sites via the formation of complexes with the pyridine nucleotides or as a result of modeling based on complexes with the ADP or P-AMP moieties of NAD^+ or $NADP^+$. In the two cases where $NADP^+$ or NAD^+ are bound, the nicotinamide is not in direct contact with the isoalloxazine ring due to presence of a conserved aromatic residue that stacks on the flavin: in *Anabaena* FNR the nicotinamide is turned toward the surface of the protein (Serre et al., 1996); in PDR it stacks on the Phe residue stacked on the flavin (Correll et al., 1992). Modeling based on the ADP complex of corn NiR (Lu et al., 1995) and the P-AMP complex of spinach FNR (Bruns & Karplus, 1995) has indicated a possible mechanism of hydride transfer in these enzymes (Karplus et al., 1991); however, the precise details of the reaction have not been established.

The structural studies have also provided insight into the nature of the interaction between the oxidoreductases and their electron transfer partners. In the PDR structure, the [2Fe-2S] cluster of the attached ferredoxin domain is in close proximity to the FMN providing a direct image of the electron transfer complex (Correll et al., 1992). Based on this structure, sequence homology, and structural comparisons of PDR, spinach FNR, and *Anabaena* 2Fe ferredoxin, a model for the interaction of spinach 2Fe ferredoxin with spinach FNR has been proposed (Correll et al., 1993). Mutants of *Anabaena* 2Fe ferredoxin at seven surface sites have been used to study the factors governing its electron transfer rate with *Anabaena* FNR (Hurley et al., 1997). The importance of electrostatic surface potential in orienting the partner proteins is inferred from calculations using the structures of B5R, NiR, spinach FNR, PDR (Nishida & Miki, 1996), and *Ec*FldR (Ingelman et al., 1997). However, with the exception of the PDR structure, structures of relevant protein:protein complexes are not yet available, and the factors controlling electron transfer in the complexes are not fully understood.

In this paper, we report the refined crystal structure of *Av*FPR, a protein that appears to use the structurally characterized FdI as its redox partner, at 2.0 Å resolution with FAD bound. The structure extends the comparative analysis of this class of oxidoreductases. It displays conserved features within the FAD and NADPH binding domains, in the folds of these domains, and in the details of the nucleotide binding sites. In addition, the structure reveals novel features in the FAD and NADPH binding sites of potential functional significance. Comparison of the structure of the *Av*FPR protein with the closely related bacterial enzyme, *Ec*FldR, that uses flavodoxin as an electron acceptor, indicates regions of *Av*FPR important for specific interaction with FdI. Knowledge of the structure provides for the first time a basis for studying in molecular detail the interaction between two partners in an oxidative stress regulatory response pathway.

Table 1. *Data collection and phasing statistics*

	Native	EMTS-1[a]	EMTS-2[a]
Unit cell parameters, Å	a = 68.36	68.04	68.10
Space group $P2_12_12$	b = 76.66	76.51	76.65
	c = 52.04	51.88	51.98
No. of crystals	1	1	1
Maximum resolution, Å	2.0	3.6	2.7
Unique reflections	19,076	2,451	7,376
Redundancy	5.0	4.3	5.2
Completeness all data, %	99.8	70.7	92.3
$R_{symm}(I)$ all data	0.101	0.109	0.081
$I/\sigma(I)$ all data	6.8	6.4	10.4
Resolution of last shell, Å	2.07–2.00	3.8–3.6	2.86–2.70
Completeness last shell, %	99.3	44.6	58.5
$R_{symm}(I)$ last shell	0.445	0.126	0.174
$I/\sigma(I)$ last shell	1.6	4.4	2.7
R_{iso}[b]	—	0.187	0.193
No. of sites	—	1	1
R_{cullis}[c]	—	0.51	0.66
Phasing power[d]	—	1.73	2.51
Figure of merit		0.50 for 7,156 reflections	

[a]EMTS, ethylmercurithiosalicylic acid, sodium salt.

[b]$R_{iso} = \Sigma||F_{ph}| - |F_p||/\Sigma|F_p|$, where $|F_{ph}|$ and $|F_p|$ are the derivative and native structure amplitudes, respectively.

[c]$R_{\text{cullis}} = \Sigma||F_{ph}(\text{calc})| - |F_p||/\Sigma|F_{ph}|$, where $|F_{ph}(\text{calc})|$ is calculated derivative structure amplitude for centric reflections.

[d]The phasing power is the ratio of the mean calculated heavy atom structure amplitude divided by the mean lack of closure error.

Results and discussion

The crystal structure of *Av*FPR has been solved using a single isomorphous Hg derivative in combination with the anomalous scattering effect (Table 1). The experimental electron density map revealed clear density for the bound FAD and was used to build a partial model of the protein. Subsequent rounds of phase combination and model building yielded a complete model for the protein (Fig. 1) (see Materials and methods). The structure has been refined at 2.0 Å resolution (Table 2).

Polypeptide chain folding and domain structure

The FPR protein is comprised of two domains, a N-terminal domain of residues 1 to 93, which binds FAD, and a C-terminal domain of residues 101 to 258, which binds $NADP^+$/NADPH (Fig. 2). The N-terminal domain contains a six-stranded all antiparallel β-barrel ($\beta1$–$\beta6$) with a capping α-helix ($\alpha1$). The FAD is bound at the crossover between the strands $\beta4$ and $\beta5$, and at the N-terminal end of helix $\alpha1$. The C-terminal domain represents a classic nucleotide binding fold with a five-stranded parallel β sheet of strand order $\beta9$-$\beta8$-$\beta7$-$\beta10$-$\beta11$. This domain contains nine helices, $\alpha2$–$\alpha10$, inserted between the β-strands. Two of the helices, $\alpha2$ and $\alpha5$, and the last turn of $\alpha6$, have 3_{10} helical parameters. By homology with known structures (below), the $NADP^+$ binding site lies across the C-terminal ends of the β-strands of the parallel sheet between $\beta7$ and $\beta10$ and includes the loop connecting $\beta7$ to $\alpha3$ and the N-terminal residues of $\alpha3$. The FAD and $NADP^+$ binding sites therefore are directly adjacent in a deep cleft formed

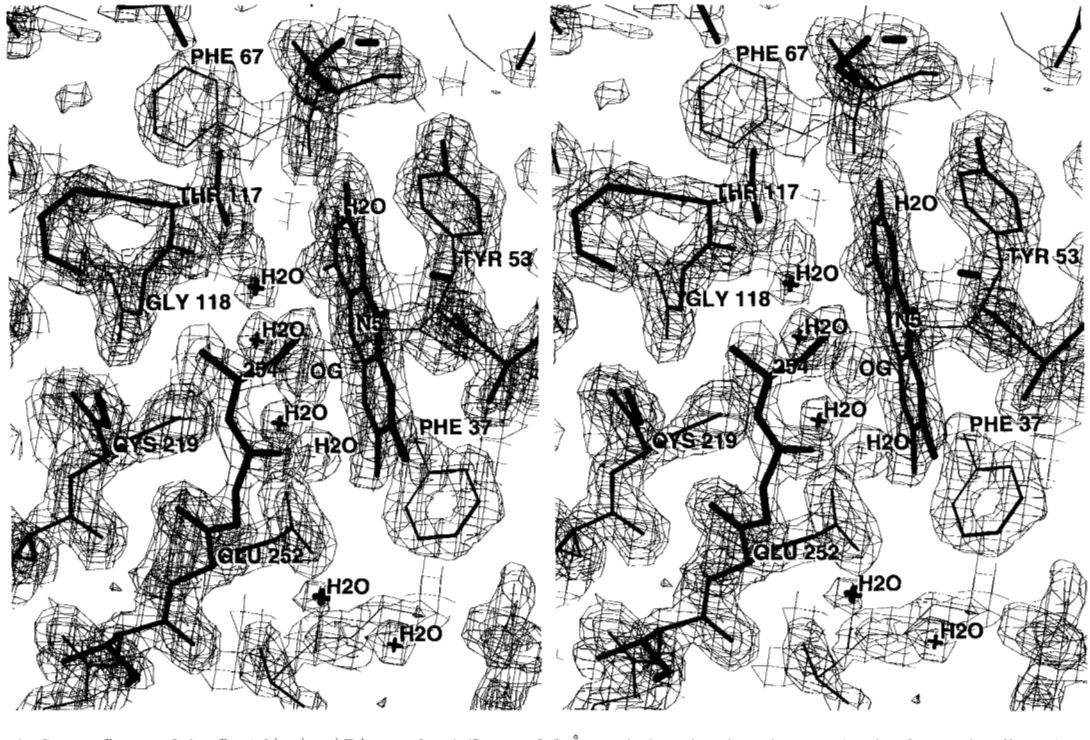

Fig. 1. Stereo figure of the final $2|F_o| - |F_c|$ map for *Av*FPR at 2.0 Å resolution showing electron density for the isoalloxazine ring of FAD, residues surrounding the flavin binding site and seven H_2O molecules which occupy the NADPH binding site. Thr117 and Gly118 are part of the GT/SGxxP motif which binds NADPH, Tyr53 is part of the RxYST motif which binds FAD, and Cys219 and Ser54 (OG) are two conserved residues on opposite sides of the NADPH binding cavity. Residue 254, which is an aromatic residue in other oxidoreductases, is an Ala in *Av*FPR. The map is contoured at 1.5 and 3.0σ.

Table 2. *Refinement statistics*

Resolution range, Å	8.0–2.0
Number of reflections	18,205
R-factor ($\|F\| > 2.0\sigma(F)$)	0.206
R-free [a]	0.262
Average *B*-factor, Å^2	
2,061 protein atoms	19.6
53 FAD atoms	19.5
85 H_2O molecules[b]	29.2
RMSD from ideality	
Bonds, Å	0.008
Angles, deg	1.53
Dihedrals, deg	25.2
Planes, deg	1.29

[a]Size of test data set 906 reflections, 5% of total.
[b]All H_2O molecules have *B*-factors < 50.0 Å^2.

by association of the two domains. The interface between the domains is mediated primarily by residues of α3 and α6 with loops of the N-terminal domain. The domains are linked by residues 94 to 100 spanning between β6 and α2. A proteolytic cleavage site observed during purification (Isas & Burgess, 1994) occurs between Ser184 and Phe185 at the extremity of the loop connecting β9 and α8 on the surface of the protein. The Hg binding site lies between the Sδ atom of Met224 and the amide nitrogen of Gly220 in the turn linking strand β10 and helix α10.

Structure comparisons

*Av*FPR and six homologous known protein structures share a common folding topology: *Ec*FldR, spinach FNR, *Anabaena* FNR, corn NiR, porcine B5R, and *Pseudomonas cepacia* PDR. A structure based alignment of the primary sequences of these proteins in comparison to *Av*FPR is given in Figure 3. In addition, the type of flavin cofactor, nicotinamide substrate, bound species (when observed), and electron transfer partner are tabulated for these oxidoreductases, as summarized in the introduction to this paper. The alignment is based on least-squares fit of Cα atoms of homologous residues after accounting for gaps and insertions. The percent sequence identity for *Av*FPR vs. the other six structures and the RMS deviations (RMSDs) of aligned Cα atoms are given in Table 3. By these criteria *Av*FPR is most homologous to *Ec*FldR and less homologous with spinach and *Anabaena* FNR, which use $NADP^+$ as a substrate rather than NADPH. By the same criteria *Av*FPR is least homologous with NiR, B5R, and PDR, consistent with the presence of a different nicotinamide substrate and/or flavin cofactor in these proteins.

As previously observed there are characteristic motifs in the sequence alignment, which correspond to functional domains (Correll et al., 1993; Lu et al., 1994; Ingelman et al., 1997). The motif RxYS/T is involved in binding the FAD or FMN, GxxT/S is involved in binding the phosphate of the FMN moiety of FAD, and

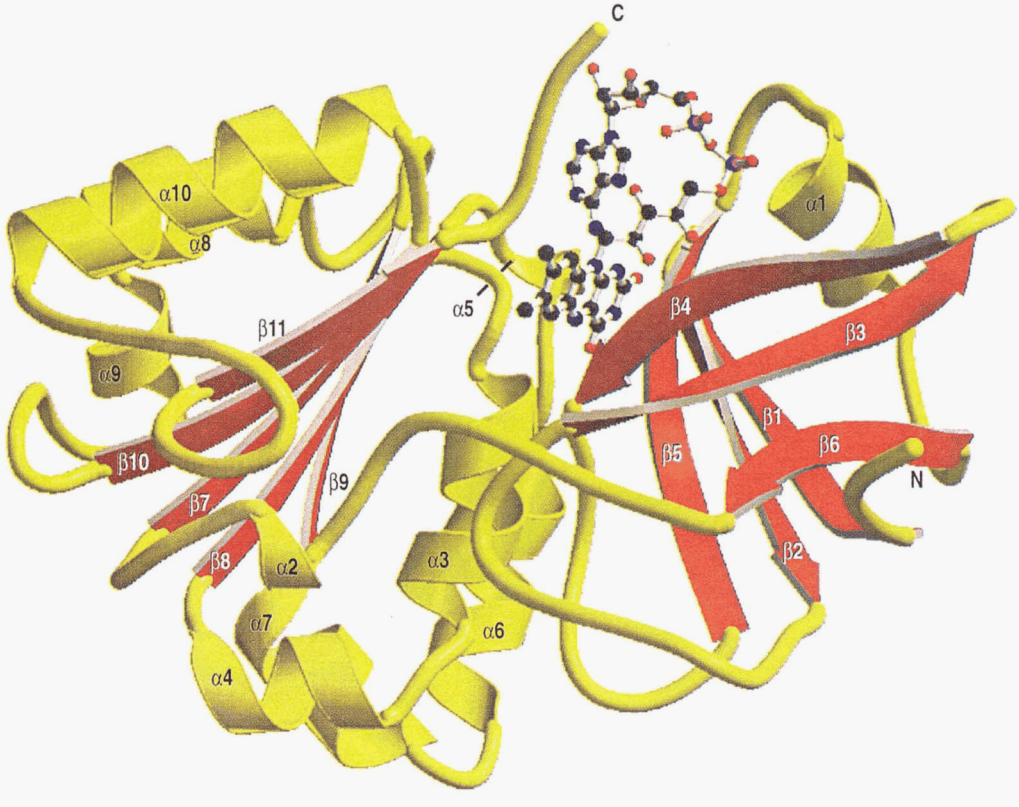

Fig. 2. The polypeptide fold of *Av*FPR with bound FAD. The β-strands and α-helices of the N-terminal (right) and C-terminal domains (left) are indicated.

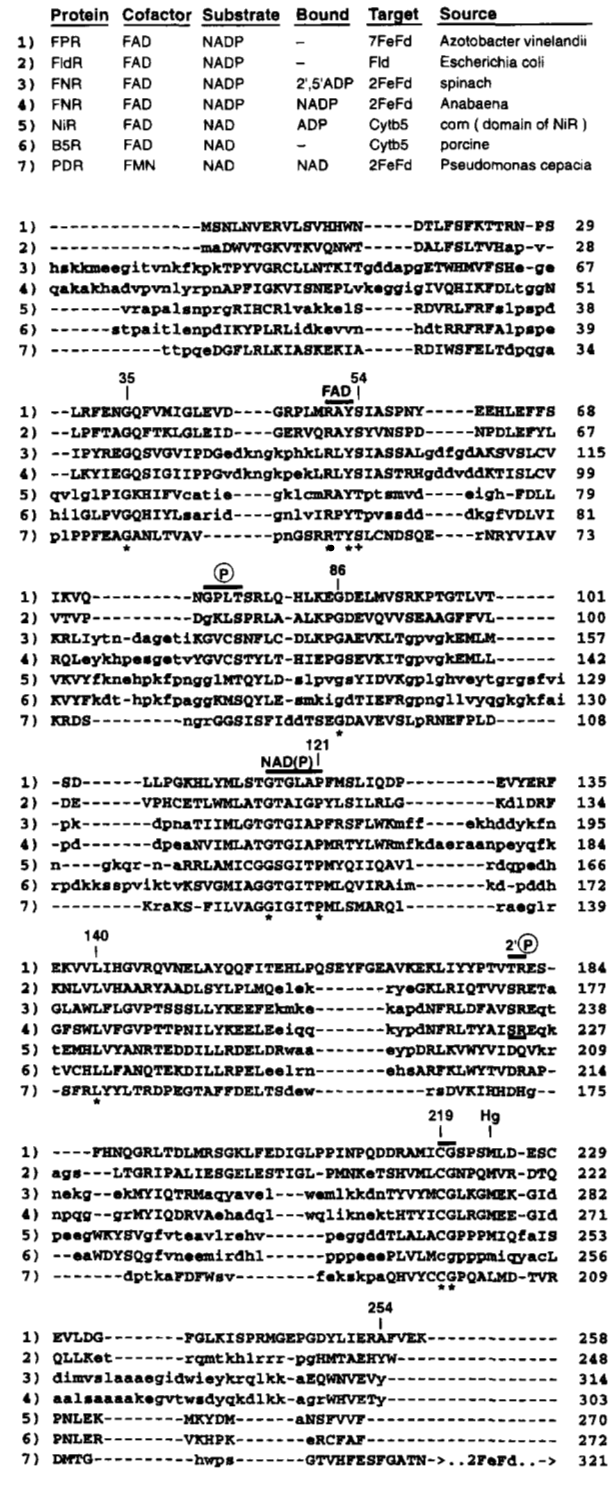

Fig. 3. Structure-based sequence alignment of *Av*FPR with six homologous oxidoreductase enzymes whose structures are known (see text). Conserved residues are indicated by an asterisk and a semiconserved Ser/Thr by a plus. Motifs are indicated by heavy lines: FAD, FAD binding motif; P, residues interacting with the FMN phosphate of FAD or FMN; NAD(P), $NADP^+/NAD^+$ binding motif; 2′P, residues defining interaction with the 2′phosphate of the 2′,5′ADP portion of $NADP^+$. Numbers above the lines correspond to residue numbers in *Av*FPR and "Hg" indicates the Met residue at the EMTS site in the Hg derivative of FPR. Lower case letters in the single character amino acid code indicate that the Cα atoms of the homologous residues are more than 3 Å apart in the two structures following least-squares superposition.

Table 3. *Comparison of AvFPR with six homologous structures*

Protein	Sequence identity (%)	Number of equivalent Cα atoms[a]	RMSD (Å)[a]
E. coli FldR	31	212	1.49
		242	2.12
Spinach FNR	17	167	1.60
		242	3.36
Anabaena FNR	18	163	1.64
		242	3.79
Corn NiR	16	139	1.97
		231	3.49
Porcine B5R	18	131	2.06
		231	3.67
P. cepacia PDR	15	143	1.71
		218	3.49

[a]For each comparison the RMSD of the matched Cα atoms is given for the number of such pairs differing by ~1.5–2.0 Å, and for a larger number of pairs representing ~90% of the *Av*FPR structure.

GxGxxP is involved in binding $NADP^+$ or NAD^+ (Fig. 3). The motif S/TR discriminates $NADP^+$ binding oxidoreductases from NAD^+ specific enzymes, which have Asp in place of the conserved Ser/Thr; the S/TR residues interact with the 2′ phosphate of the 2′,5′ ADP portion of $NADP^+$ (Bruns & Karplus, 1995). Two conserved residues, Ser/Thr in RxYS/T and Cys in CG (residues 54 and 219 in *Av*FPR), lie on either side of the the $NAD^+/NADP^+$ binding site and are thought to be involved in catalysis (Correll et al., 1993). In *Av*FPR the side chains of these residues are 5.2 Å apart and are oriented toward a cavity that is adjacent to the isoalloxazine ring of FAD and occupied by five water molecules. Three additional conserved residues, Gly35, Gly86, and Leu140 in *Av*FPR, are not involved in the nucleotide binding sites; presumably they are required for folding or stability of the domains. Gly35 precedes strand β3, Gly86 precedes strand β6, and Leu140 is buried in the hydrophobic core of the C-terminal domain.

A superposition of *Av*FPR and *Ec*FldR, two closely related bacterial reductases, is shown in Figure 4 in the same orientation as in Figure 2. The superposition is based on least-squares fit of homologous pairs of Cα positions in the structures and in the primary sequence alignment (Fig. 3; Table 3). It is possible to more perfectly align either the β-barrels of the N-terminal domains or the parallel β-sheets of the C-terminal domains, but not both simultaneously, indicating a small difference in the disposition of the two domains with respect to each other in the two structures. Even though the *A.vinelandii* protein is 10 residues longer in primary sequence the two structures are very similar. There are three main regions of difference: at the C-terminus of *Av*FPR which is extended by three amino acids (residues 256–258) adjacent to the FAD binding site; at residues 185–186 in *Av*FPR and 177–180 in *Ec*FldR which are part of a loop following the β9 strand on the "back" side of the C-terminal domain; and at residues 162–168 in *Av*FPR which comprise a seven residue insertion in a loop at the "bottom" of the C-terminal domain. This later insertion is unique to *Av*FPR vs. the other proteins of known structure (Fig. 3). Additional single amino acid insertions occur at residues 29, 207, and 245 in *Av*FPR and at residue 228 in *Ec*FldR. The larger differences, especially additional residues adjacent to FAD in *Av*FPR, may be significant in defining the interaction of FPR with 7Fe ferredoxin vs. *Ec*FldR with flavodoxin.

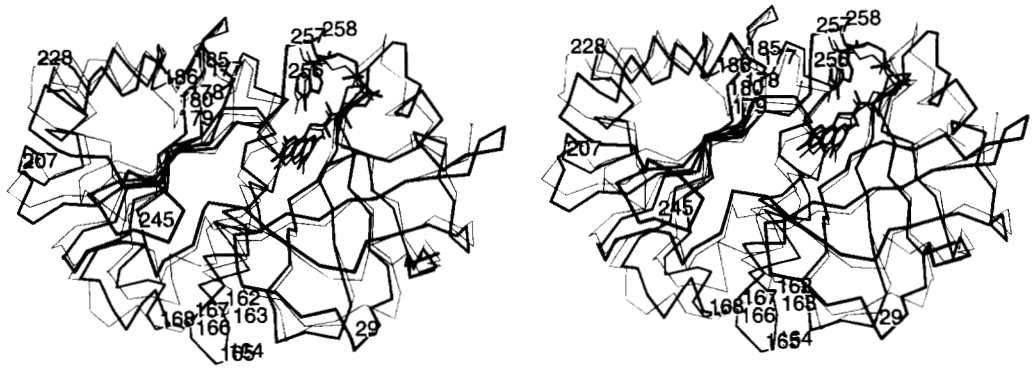

Fig. 4. Stereo figure of the superposition of *Av*FPR (thick lines) and *Ec*FldR (thin lines) based on least-squares fit of homologous residues. Only the Cα atoms and bound FAD in each structure are shown. Residues corresponding to insertions, deletions, or additions in the sequence alignment (Fig. 3) are labeled indicating local regions of difference between the two structures. The view is the same as in Figure 2. Residue 1 is disordered in both structures and residues 44–46 are not ordered in *Ec*FldR.

FAD binding and conformation

The conformation of the FAD in *Av*FPR and its local environment is shown in Figure 5. The cofactor is bound by the N-terminal domain in a manner similar to other flavin binding domains (Murzin, 1998). The FMN moeity interacts with residues of the β4 and β5 strands while the phosphate is positioned at the N-terminus of the short α-helix that caps the β-barrel (Fig. 2). In addition to the positive electrostatic dipole provided by this helix, the FMN phosphate negative charge is balanced by hydrogen bonds from the amides of Leu76 and Thr77 in the GxxT/S motif within the helix. Residues in the RxYS/T motif on strand β4 have several contacts to the FAD: Arg51 provides a charged hydrogen bond to the FMN phosphate, Ala52 hydrogen bonds with the ribityl C2′ hydroxyl group, and Tyr53 stacks on the isoalloxazine ring. Residues on the β5 strand provide complementary hydrogen bonds to the N3 and

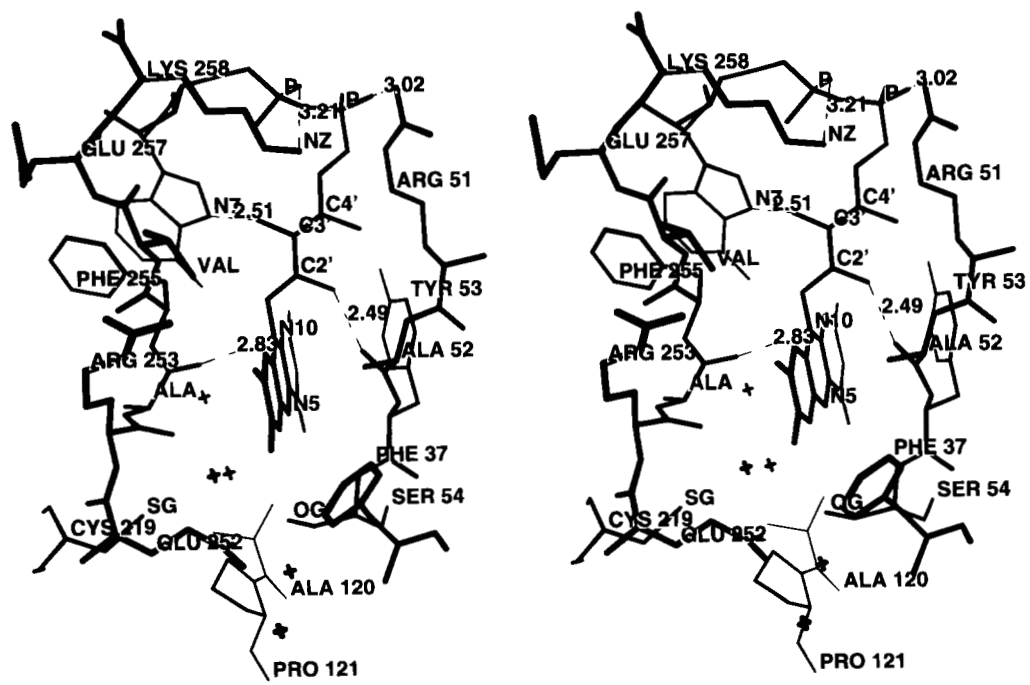

Fig. 5. Stereo figure of the local environment of FAD in *Av*FPR showing residues 51–54 of the RxYS/T motif, Phe37, residues 252–258, which include a unique C-terminal extension, Cys219 and residues 120, 121 of the GT/SGxxP motif. Tyr53 and Phe255 are involved in stacking interactions with the isoalloxazine and adenine rings of FAD, respectively. Ala254 is an aromatic residue in the *Ec*FldR and FNR enzymes. Water molecules (crosses) occupy the NADPH binding site adjacent to the flavin. The conserved residues Ser54 and Cys219 lie on either side of this cavity. Possible hydrogen bonds are indicated with distances in Å. Each phosphate of FAD interacts with a basic residue and the carbonyl oxygen of Ala254 is adjacent to N10 of the flavin. Not shown are the residues of the helix α1 whose N-terminal dipole is oriented toward the phosphates, and specific hydrogen bonds between O2 and N3 of the flavin and residues on strand β5.

O2 atoms of the isoalloxazine ring (carbonyl of Phe67 and amide of Ile69, respectively) and also hydrogen bond with Tyr53 (side chain of Ser68). The O4 and N5 atoms of the ring interact with water molecules occupying the NADPH site adjacent to the conserved residues Ser54 and Cys219 (Figs. 1, 5). The C7 methyl group of the dimethylbenzene portion of the ring is in close contact with Phe37, but the C8 methyl group is exposed to solvent at the edge of the binding pocket. Contacts to the AMP portion of FAD are provided by residues in the C-terminal domain. In particular, Phe255 stacks directly on the adenine ring and the C-terminal Lys258 side chain provides a charged hydrogen bond to the AMP phosphate. Consequently, the FMN and AMP halves of the FAD are bound to the *Av*FPR protein through contacts that involve primarily the N- and C-terminal domains, respectively. Together these interactions provide charge neutralization of both phosphates, aromatic stacking with both rings and complementary hydrogen bond recognition as well as nonpolar contacts.

The FAD cofactor adopts two distinct conformations in the four proteins, which utilize NADPH/$NADP^+$ (Fig. 3). In the bacterial *Av*FPR and *Ec*FldR enzymes, the AMP portion is folded back placing the adenine and isoalloxazine rings in proximity (Figs. 4, 5), whereas in spinach and *Anabaena* FNR the cofactor is extended so that the adenine ring is distal from the isoalloxazine ring. The driving force for these two conformations appears to be aromatic stacking. In *Av*FPR the adenine stacks on Phe255 (Fig. 5) and in *Ec*FldR it interacts with the side chain of the homologous, C-terminal Trp248 residue. Averaged over all 53 atoms, the superposed FAD cofactors in FPR and FldR differ by 0.91 Å. Spinach and *Anabeana* FNR lack an aromatic residue homologous to Phe255 or Trp248. In these enzymes the adenine of FAD is oriented toward the solvent while stacking on a Tyr side chain in the N-terminal domain (residues 120 and 104 in spinach and *Anabaena*, respectively). Although the AMP halves of FAD adopt different conformations, the FMN portions exhibit very similar conformations when the four homologous proteins are superposed. However, there is one distinct difference in the ribityl chain in *Av*FPR. In this case the hydroxyl groups on C3′ and C4′ are rotated by approximately 45 and 90°, respectively, relative to the other ribityl chains. This conformation allows for a potential interaction between the C3′ hydroxyl and N7 of adenine (Fig. 5), but it does not allow for a hydrogen bond between the C4′ hydroxyl and Tyr53 in the RxYS/T motif as observed in *Ec*FldR and both FNR enzymes.

Unique features of AvFPR

A unique aspect of the environment of FAD in *Av*FPR is the absence of an aromatic residue stacked on the isoalloxazine ring in the NADPH binding pocket. In *Ec*FldR, spinach FNR and *Anabaena* FNR Tyr247, Tyr314, and Tyr303 (Fig. 3), respectively, lie directly adjacent to the isoalloxazine ring. This ring is in turn in contact on its opposite face with the Tyr of the RxYS/T motif in a very similar edgewise manner in each structure. In contrast, in *Av*FPR the residue homologous to the C-terminal Tyr of the other structures is Ala254 so that there is no aromatic interaction on this face of the isoalloxazine ring. Furthermore, the main-chain conformation differs due to additional C-terminal residues so that the methyl group of Ala254 is directed away from the isoalloxazine ring while the carbonyl of this residue is normal to the ring and only 2.8 Å from N10 (Fig. 5). The lack of an aromatic residue may be compensated by a more direct stacking interaction on the opposite face of the flavin. Tyr53 in the RxYS/T motif is more nearly parallel with the isoalloxazine ring (Fig. 5) than in the other structures, perhaps due to the alternate interactions of Tyr53 with Ser68 but not with the ribityl C4′ hydroxyl. In *Av*FPR the angle between the two aromatic rings is 30° whereas in *Ec*FldR, spinach FNR and *Anabaena* FNR it is 45–55°.

The absence of an aromatic residue stacked on the isoalloxazine ring of FAD may be functionally significant. As noted, in three homologous structures a Tyr is stacked on the flavin ring, requiring that it be displaced for productive interaction between the nicotinamide and FAD. Further, the energy required to displace this residue must be significant because in the available structures of complexes with $NADP^+$ and NAD^+ the aromatic residue remains in place. Specifically, in the $NADP^+$ complex of *Anabaena* FNR, Tyr303 occupies the active site and the nicotinamide portion of $NADP^+$ is turned away and lies on the surface of the protein about 15 Å from the flavin ring (Serre et al., 1996). In the structure of the NAD^+ complex of PDR, the side chain of Phe225 is in the "gate-closed" position where it is stacked between the flavin and nicotinamide rings (Correll et al., 1992). Similarly, in the structure of cytochrome P450 reductase, which contains $NADP^+$ and FAD binding domains homologous to those in *Av*FPR and FNRs as well as a FMN binding domain, Trp677 is stacked on the FAD flavin while the $NADP^+$ nicotinamide ring is nearby but disordered (Wang et al., 1997). Therefore, the fact that there is no aromatic residue to be displaced in *Av*FPR could be expected to favor the binding of NADPH and presumably to accelerate the rate of reduction of FAD. Nevertheless, in spite of the lack of an aromatic residue to interfere with $NADP^+$ binding, it has not yet been possible to soak crystals in $NADP^+$ without loss of crystalline order.

Another unique aspect of the occurrence of Ala254 in *Av*FPR is the proximity of the carbonyl of this residue to the N10 atom of the isoalloxazine ring (Fig. 5). A carbonyl in this position should not interfere with interaction of nicotinamide with the N5 or N1 positions of the ring. Also, the carbonyl oxygen is 5.8 and 6.4 Å, respectively, from the conserved Cys219 and Ser54 side chains, which may participate in catalysis (Correll et al., 1993). A negatively charged dipole oriented directly toward the π orbitals of the aromatic ring system might be expected to alter the electronic properties of the isoalloxazine ring, and perhaps could account for the absence of a stable semiquinone state in *Av*FPR (Isas & Burgess, 1994).

If the presence of Ala254 in *Av*FPR is functionally significant then it would be predicted to be conserved. A number of species contain ferredoxins homologous to FdI; among them the *Pseudomonas* sp. show the greatest homology (Iismaa et al., 1991). Recently, the genome of the human pathogen *Pseudomonas aeruginosa* has been sequenced. A database search reveals that *P. aeruginosa* contains a 7Fe ferredoxin with 93% sequence identity to *A. vinelandii* FdI and so could be expected to contain a FPR-like protein as well. Indeed, the sequence of an FPR-like protein in *P. aeruginosa* is 85% identical and 91% similar to *Av*FPR. Further, in the putative *P. aeruginosa* FPR protein there is an Ala at the position of Ala254 and the following C-terminal residues are identical as well (PheValGluLys).

A further significant difference in the environment of the FAD in *Av*FPR compared to the other $NADP^+$ or NAD^+ utilizing enzymes is due to the three residue C-terminal extension (Fig. 3), which includes Lys258 at the C-terminus. Consequently, Lys258 and Arg51 in the RxYS/T motif together provide charged hydrogen bonds to both phosphate groups of FAD (Fig. 5). In contrast, the Arg in the RxYS/T motif in five other FAD containing en-

zymes is the only basic residue to interact with the FAD phosphates, aside from the N-terminal domain helix dipole. The presence of two basic groups in contact with the FAD in *Av*FPR alters the electrostatic environment and may affect the rate of electron transfer with 7Fe ferredoxin. In *Av*FPR there are also 10 Arg and Lys residues on the surface of the protein surrounding the NADPH and FAD binding cleft, in addition to Arg51 and Lys258: Lys70, Arg79, Arg145, Arg182, Arg190, Arg196, Lys199, Lys238, Arg242, and Arg253. Clustering of basic residues on the protein surface near the active site has also been observed in the structures of *Ec*FldR (Ingelman et al., 1997), spinach FNR (Bruns & Karplus, 1995), and *Anabaena* FNR (Serre et al., 1996). A detailed analysis of the interaction of FPR with FdI (Y.-S. Jung & B.K. Burgess, unpubl. results) considering the electrostatic potential surfaces of the two proteins will be presented separately.

Materials and methods

A. vinelandii NADPH:ferredoxin oxidoreductase (FPR) was purified (Isas & Burgess, 1994; Isas et al., 1995) and crystallized (Diller et al., 1994) as previously described, except that the polyethylene glycol 4000 precipitant in the reservoir solutions was replaced with 1.0 M sodium citrate, pH 5.5. Crystals grown in this way are isomorphous to those grown from polyethylene glycol 4000 (Table 1). Crystals were mounted in thin-walled glass capillaries using the reservoir solution as a synthetic mother liquor and data were collected at 18 °C. Native data were collected using CuKα radiation from a Siemens SRA rotating anode X-ray generator operated at 50 kV, 100 mA, and equipped with a graphite monochromator. The data were recorded with a Mar-Research 30 cm diameter image plate scanner and processed with Mosflm and the CCP4 suite of programs (Leslie, 1994) (Table 1).

Molecular replacement calculations using models based on the structures of spinach FNR (Bruns & Karplus, 1995) and *E. coli* flavodoxin reductase (Ingelman et al., 1997) were not successful. Approximately 50 heavy atom compounds were screened for derivatives without success. However, crystals soaked in ethylmercurithiosalicylic acid (EMTS) yielded a single site derivative. Crystals were soaked for 18 h at 25 °C in a reservoir solution containing 0.5 mM EMTS. Crystals were mounted as for the native crystals and data were collected at 18 °C. Derivative data sets were collected using CuKα radiation from a Rigaku RU200 rotating anode X-ray generator operated at 40 kV, 80 mA, and equipped with a graphite monochromator. The data were recorded with a Siemens X-1000 (Xentronics) multiwire area detector and processed with the Xengen suite of programs (Howard et al., 1985) (Table 1). Complete native and derivative data sets were also collected at 100 K at Stanford Synchrotron Radiation Laboratory beamline 9-1 at a wavelength of 0.77 Å (data not shown). However, the EMTS derivative is not isomorphous at this temperature.

The isomorphous and anomalous difference Patterson maps computed with the Xtalview suite of programs (McRee, 1992) using the room temperature native and both EMTS data sets contained, respectively, 15σ and 5σ peaks in each of the three Harker sections for each derivative consistent with a single Hg site. The site was refined against each data set and isomorphous replacement with anomalous scattering phases were calculated to 2.7 Å resolution with the MLPHARE and CCP4 programs (Leslie, 1994) (Table 1). The electron density map was improved by solvent flattening and histogram matching using DM and the phases were extended to 2.5 Å (Cowtan, 1994). The map revealed clear density for strands of the parallel β sheets in the protein. These and connecting residues were modeled as polyalanine segments using Xfit (McRee, 1992). Phases derived from a partial model comprising 120 alanine residues were combined with the 2.5 Å experimental phases using SIGMAA (Read, 1986). The resulting electron density map permitted modeling of another 120 alanine residues in a nearly complete chain trace. Phase combination based on this model led to a map in which the entire structure with side chains could be interpreted in agreement with the primary sequence (Isas et al., 1995). The FAD cofactor was modeled in the experimental 2.5 Å map.

The model was refined with Xplor version 3.8 (Brünger et al., 1989) using simulated annealing at 2.5 Å resolution, and subsequently at 2.25 and 2.0 Å. The free *R*-value was used for assessing the progress of refinement (Brünger, 1992). Corrections and adjustments to the model were made following each stage of refinement using $2|F_o| - |F_c|$ maps calculated with all data in the range 20.0 Å to the limiting resolution. Isotropic *B*-factors were refined for all protein and FAD atoms. Water molecules were interpreted from difference Fourier maps for 3σ peaks within 3.5 Å of polar protein atoms and retained in the model if their refined *B*-factors were less than 50.0 Å^2. The final model refined against all data in the resolution range 8.0–2.0 Å is comprised of 2,199 atoms for residues 2 to 258 of the protein, FAD, and 85 solvent atoms (Met1 at the N terminus is disordered). Statistics for the refinement are summarized in Table 2. In the final model there are no outliers in the Ramachandran plot and residues Gly74–Pro75 form a *cis*-peptide linkage. Coordinates have been deposited with the Protein Data Bank with accession code 1A8P. Images of the structure have been rendered using Xfit (McRee, 1992), Molscript (Kraulis, 1991), and Raster3D (Merritt & Murphy, 1994).

Acknowledgments

We sincerely thank the following people: Chris Bruns for assistance with sequence alignments using his program CKWHENCE, for coordinates of spinach FNR and for structural interpretation; Pamela Williams for assistance in data collection; Duncan McRee for advice on MIR phase calculations; Hans Eklund and colleagues for coordinates of *E. coli* flavodoxin reductase prior to release by the PDB; and Julieann Grant for technical assistance. This research was supported by National Institutes of Health grants GM36325 to C.D.S. and GM45209 to B.K.B.

References

Bianchi V, Reichard P, Eliasson R, Pontis E, Krook M, Jornvall H, Haggard-Ljungquist E. 1993. *Escherichia coli* ferredoxin NADP$^+$ reductase: Activation of *E. coli* anaerobic ribonucleotide reduction, cloning of the gene (fpr), and overexpression of the protein. *J Bacteriol 175*:1590–1595.

Brünger AT. 1992. Free *R* value: A novel statistical quantity for assessing the accuracy of crystal structures. *Nature 355*:472–475.

Brünger AT, Karplus M, Petsko GA. 1989. Crystallographic refinement by simulated annealing: Application to crambin. *Acta Crystallogr A45*:50–61.

Bruns CM, Karplus AP. 1995. Refined crystal structure of spinach ferredoxin reductase at 1.7 Å resolution: Oxidized, reduced and 2′-phospho-5′-AMP bound states. *J Mol Biol 247*:125–145.

Correll CC, Batie CJ, Ballou DP, Ludwig ML. 1992. Phthalate dioxygenase reductase: A modular structure for electron transfer from pyridine nucleotides to [2Fe-2S]. *Science 258*:1604–1610.

Correll CC, Ludwig ML, Bruns CM, Karplus PA. 1993. Structural prototypes for an extended family of flavoprotein reductases: Comparison of phthalate dioxygenase reductase with ferredoxin reductase and ferredoxin. *Protein Sci 2*:2112–2133.

Cowtan K. 1994. The CCP4 suite: Programs for protein crystallography. *Acta Crystallogr D50*:760–763.

Diller TC, Shaw A, Isas JM, Burgess BK, Stout CD. 1994. Diffraction quality crystals of protein X from *Azotobacter vinelandii*. *J Mol Biol 241*:620–621.

Howard AJ, Nielsen C, Xuong NH. 1985. Software for a diffractometer with multiwire area detector. *Methods Enzymol 114A*:452–472.

Hurley JK, Weber-Main AM, Stankovich MT, Benning MM, Thoden JB, Vanhooke JL, Holden HM, Kee Chae Y, Xia B, Cheng H, Markley JL, Martinez-Julvez M, Gomez-Moreno C, Schmeits JL, Tollin G. 1997. Structure-function relationships in *Anabaena* ferredoxin: Correlations between X-ray crystal structures, reduction potentials, and rate constants of electron transfer to ferredoxin: $NADP^+$ reductase for site-specific ferredoxin mutants. *Biochemistry 36*:11100–11117.

Iismaa SE, Vasquez AE, Jensen GM, Stephens PJ, Butt JN, Armstrong FA, Burgess BK. 1991. Site directed mutagenesis of *Azotobacter vinelandii* ferredoxin I: Changes in [4Fe-4S] cluster reduction potential and reactivity. *J Biol Chem 266*:21563–21571.

Ingelman M, Bianchi V, Eklund H. 1997. The three-dimensional structure of flavodoxin reductase from *Escherichia coli* at 1.7 Å resolution. *J Mol Biol 268*:147–157.

Isas JM, Burgess BK. 1994. Purification and characterization of a $NADP^+$/NADPH-specific flavoprotein that is overexpressed in FdI^- strains of *Azotobacter vinelandii*. *J Biol Chem 269*:19404–19409.

Isas JM, Yannone SM, Burgess BK. 1995. *Azotobacter vinelandii* NADPH: Ferredoxin reductase cloning, sequencing and overexpression. *J Biol Chem 270*:21258–21263.

Karplus PA, Daniels MJ, Herriott JR. 1991. Atomic structure of ferredoxin-$NADP^+$ reductase: Prototype for structurally novel flavoenzyme family. *Science 251*:60–66.

Kraulis PJ. 1991. Molscript: A program to produce both detailed and schematic plots of protein structures. *J Appl Cryst 24*:946–950.

Leslie AGW. 1994. The CCP4 suite: Programs for protein crystallography. *Acta Crystallogr D50*:760–763.

Liochev SI, Hausladen A, Beyer WF, Fridovich I. 1994. NADPH:ferredoxin oxidoreductase acts as a paraquat diaphorase and is a member of the soxRS regulon. *Proc Natl Acad Sci 91*:1328–1331.

Lu G, Campbell WH, Schneider G, Lindqvist Y. 1994. Crystal structure of the FAD-containing fragment of corn nitrate reductase at 2.5 Å resolution: Relationship to other flavoprotein reductases. *Structure 2*:809–821.

Lu G, Lindqvist Y, Schneider G, Dwivedi U, Campbell W. 1995. Structural studies on corn nitrate reductase: Refined structure of the cytochrome *b* reductase fragment at 2.5 Å, its ADP complex and an active-site mutant and modeling of the cytochrome *b* domain. *J Mol Biol 248*:931–948.

McRee DE. 1992. A visual protein crystallographic software system for XII/Xview. *J Mol Graphics 10*:44–47.

Merritt EA, Murphy MEP. 1994. Raster 3D Version 2.0: A program for photorealistic molecular graphics. *Acta Cryst D50*:869–873.

Morgan TV, Lundell DJ, Burgess BK. 1988. *Azotobacter vinelandii* ferredoxin I: Cloning, sequencing, and mutant analysis. J *Biol Chem 263*:1370–1375.

Murzin AG. 1998. Probable circular permutation in the flavin-binding domain. *Nat Struct Biol 5*:101.

Nishida H, Inaka K, Yamanaka M, Kaida S, Kobayashi K, Miki K. 1995. Crystal structure of NADH-cytochrome b5 reductase from pig liver at 2.4 Å resolution. *Biochemistry 34*:2763–2767.

Nishida H, Miki K. 1996. Electrostatic properties deduced from refined structures of NADH-cytochrome b5 reductase and the other flavin-dependent reductases: Pyridine nucleotide-binding and interaction with an electron-transfer partner. *Proteins Struct Funct Genet 26*:32–41.

Read RJ. 1986. Improved Fourier coefficients for maps using phases from partial structures with errors. *Acta Cryst A42*:140–149.

Serre L, Vellieux FMD, Medina M, Gomez-Moreno C, Fontecilla-Camps JC, Frey M. 1996. X-ray structure of the ferredoxin: NADP reductase from the cyanobacterium *Anabaena* PCC 7119 at 1.8 Å resolution and crystallographic studies of $NADP^+$ binding at 2.25 Å resolution. *J Mol Biol 263*: 20–39.

Stout CD. 1989. Refinement of the 7 Fe ferredoxin from *Azotobacter vinelandii* at 1.9 Å resolution. *J Mol Biol 205*:545–555.

Yannone SM, Burgess BK. 1997. Identification of a palindromic sequence that is responsible for the up-regulation of NADPH-ferredoxin reductase in a ferredoxin I deletion strain of *Azotobacter vinelandii*. *J Biol Chem 272*:14454–14458.

Yannone ST, Burgess BK. 1998. The seven iron FdI from *Azotobacter vinelandii* regulates the expression of NADPH: Ferredoxin reductase via an oxidative stress response. *J Biol Inorg Chem*. Forthcoming.

Wang M, Roberts DL, Paschke R, Shea TM, Masters BSS, Kim JJP. 1997. Three dimensional structure of NADPH-cytochrome P450 reductase: Prototype for FMN and FAD containing enzymes. *Proc Natl Acad Sci 94*:8411–8416.